Med Biol Eng Comput (2008) 46:671–679
DOI 10.1007/s11517-008-0316-0

ORIGINAL ARTICLE

Parallel implementation of the accelerated BEM approach for EMSI of the human brain

Y. Ataseven · Z. Akalın-Acar · C. E. Acar · N. G. Gençer

Received: 27 June 2007 / Accepted: 5 February 2008 / Published online: 26 February 2008

Abstract Boundary element method (BEM) is one of the numerical methods which is commonly used to solve the forward problem (FP) of electro-magnetic source imaging with realistic head geometries. Application of BEM generates large systems of linear equations with dense matrices. Generation and solution of these matrix equations are time and memory consuming. This study presents a relatively cheap and effective solution for parallel implementation of the BEM to reduce the processing times to clinically acceptable values. This is achieved using a parallel cluster of personal computers on a local area network. We used eight workstations and implemented a parallel version of the accelerated BEM approach that distributes the computation and the BEM matrix efficiently to the processors. The performance of the solver is evaluated in terms of the CPU operations and memory usage for different number of processors. Once the transfer matrix is computed, for a 12,294 node mesh, a single FP solution takes 676 ms on a single processor and 72 ms on eight processors. It was observed that workstation clusters are cost effective tools for solving the complex BEM models in a clinically acceptable time.

Keywords Electro-magnetic source imaging (EMSI) · Boundary element method · BEM · Forward problem · Parallel processing · Beowulf cluster · Human brain · SIMD · PETSc · MPI · BLAS · ATLAS

Y. Ataseven · Z. Akalın-Acar · C. E. Acar · N. G. Gençer (✉)
Department of Electrical and Electronics Engineering,
Brain Research Laboratory, Middle East Technical University,
06531 Ankara, Turkey
e-mail: ngencer@metu.edu.tr

Y. Ataseven
e-mail: yoldas@eee.metu.edu.tr

Z. Akalın-Acar
e-mail: zakalin@gmail.com

C. E. Acar
e-mail: canacar@gmail.com

1 Introduction

In electro-magnetic source imaging (EMSI), the aim is to determine the distribution of the electrical activity inside the brain using the electroencephalography (EEG) and magnetoencephalography (MEG) measurements [4, 15, 19, 26, 35, 39]. The forward problem (FP) of EMSI is defined as calculating the electric potentials/magnetic fields on/near the scalp surface, given the electrical activities in the brain [16]. The inverse problem (IP) is defined as finding the electrical activities from these measurements. It is apparent that accurate results require accurate modeling [13, 14, 34]. Since analytical solutions for the FP are not available for realistic head models, numerical methods are employed. Boundary element method (BEM) is a numerical method that solves the electric potentials and magnetic fields on the boundaries of different conductivity regions [13, 14, 18, 27, 29, 34, 36]. In the BEM formulation, the integral equations on the boundaries are discretized to form a linear system of equations. However, when realistic head models are used, generation and solution of the resulting equation is computationally expensive. The purpose of this study is to present a scalable parallelization scheme using a Beowulf cluster [11]. The advantages of such a system are twofold: speeding up the FP calculations and elimination of the memory limitations.

Computational complexity is a limiting factor that prevents the use of detailed BEM models. In order to avoid long processing times and to prevent running out of memory, even the recent studies use coarse meshes for realistic models [17]. Recent work by Akalın-Acar and Gençer [2], introduced the accelerated BEM formulation for EEG and MEG in order to speed-up the FP solutions. Accelerated BEM formulation computes transfer matrices from the BEM system matrix (coefficient matrix) and electrode/sensor positions. Once these matrices are computed, the FP solutions are reduced to simple matrix-vector multiplications. Unfortunately, even with accelerated BEM approach, the pre-computation phase takes a long time for detailed meshes, and the transfer matrices require additional memory.

Parallel processing is one way of reducing the computational requirements of a computationally complex problem. Parallel implementation of the BEM was previously used to solve various engineering problems [6, 37, 44]. While there is no parallel implementation of BEM for the EMSI FP, there are several studies that used parallel processing with the finite element method (FEM) to solve the FP of EMSI [1, 20, 47].

For a parallel implementation of EMSI using BEM, the algorithms must be chosen according to the requirements of the formulations and the problem. The BEM system matrix is large, and has no special properties such as symmetry and positive-defineteness. Furthermore, the required number of solutions (number of sensors) is small compared to the size of the matrix. Therefore, it is not feasible to use direct (Gauss elimination based) solution methods. Instead, iterative methods can be applied.

Iterative methods are divided into two main groups: stationary methods and Krylov subspace methods (KSMs) [10]. It has been shown that, for the BEM, there are efficient robust iterative KSMs which are better than the Gauss-based methods in complexity [30] and thus in processing time. They are also superior to stationary methods in convergence rate.

In this study, a workstation cluster of eight computers is used as a computational platform [11]. To solve the system of equations, the portable, extensible toolkit for scientific computation (PETSc) [5] is employed which allows the use of almost all KSMs in the literature. Using this framework, a parallelization scheme is proposed to solve the FP of EMSI using the accelerated BEM.

The paper will proceed as follows: first, a general overview of the BEM and its computational aspects are presented. Next, the proposed parallelization scheme is introduced. Finally, the performance of different KSMs in the solution of the BEM equation is assessed and the speed-up provided by the parallelization scheme is reported.

2 Methods

2.1 Overview of the boundary element method

The BEM is a numerical method that models the boundaries between regions of uniform conductivity. The FP of EMSI can be expressed in terms of the surface integrals over these boundaries, and BEM uses triangular surfaces to discretize the problem and expresses it in terms of a matrix equation. The matrix Eq. (1) provides the relationship between unknown surface potentials and a source term:

$$\mathbf{A}\Phi = \mathbf{g} \tag{1}$$

where Φ is a vector of node potentials, $\mathbf{A}$ is a matrix whose elements are determined by the geometry and electrical conductivity of the head and $\mathbf{g}$ is a vector representing the contribution of the primary sources.

When the node potentials are computed, the magnetic field at a given sensor position can be obtained from these potentials by:

$$\mathbf{B} = \mathbf{B_0} + \mathbf{H}\Phi \tag{2}$$

here, $\mathbf{B}$ is a vector representing the magnetic fields at the sensor locations. The vector $\mathbf{B_0}$ is the magnetic field at the same sensor locations due to the same sources in an unbounded homogenous medium. The $\mathbf{H}$ matrix is a coefficient matrix determined by the geometry and electrical conductivity of the head.

When solving the BEM matrix, the significant conductivity difference between the brain and the skull may cause numerical instability [29]. This instability can be overcome by computing a correction term (Φ_3^0) for the right-hand-side of the matrix equation. This technique is called the isolated problem approach (IPA) [22, 29].

When solving the IP, it is sufficient to solve the FP at the sensor locations. Accelerated BEM [2] generates a transfer matrix describing the relationship between the sensors and the sources. Using the transfer matrix, the sensor potentials/magnetic fields are obtained by a simple matrix-vector multiplication:

$$\begin{aligned}\Phi_e &= \mathbf{D}\Phi = \mathbf{D}\mathbf{A}^{-1}\mathbf{g} \\ &= \mathbf{E}\mathbf{g}\end{aligned} \tag{3}$$

where $\mathbf{D}$ is sparse matrix that describes each electrode potential in terms of node potentials. Since the number of sensors (m) is much less than the number of nodes, it is much faster to solve the following equation for each column of $\mathbf{E}$:

$$\mathbf{A}^{\mathbf{T}}\mathbf{e_i} = \mathbf{d_i} \tag{4}$$

Similarly, for the MEG,

$$\begin{aligned}\mathbf{B} &= \mathbf{B_0} + \mathbf{H}\mathbf{A}^{-1}\mathbf{g} \\ &= \mathbf{B_0} + \mathbf{M}\mathbf{g}\end{aligned} \tag{5}$$

and

$$\mathbf{A}^T\mathbf{m}_i = \mathbf{h}_i \tag{6}$$

After computing the transfer matrix **E**, the FP solution for a given source reduces to calculating **g** for that source and performing a matrix-vector multiplication.

The details of the BEM formulation were described in [2, 21, 22] and are summarized in the Appendix.

2.2 Computational complexity

2.2.1 Accelerated BEM for EEG

To obtain the EEG transfer matrix **E**, one must first calculate the coefficient matrix **A** in Eq. (1). Each row of **A** is calculated by visiting all elements of the mesh for surface integration. On each element, the surface integral is approximated by a weighted sum of potentials at the Gauss–Legendre quadrature points [12, 21]. For elements close to the field node, recursive integration [17] is used for better accuracy.

The number of floating point operations (*flops*) is then proportional to $N \times E \times N_{\text{gp}} \times N_{\text{npe}} \times C_{\text{int}}$, where N is the number of nodes, E is the number of elements, N_{gp} is the number of Gauss–Legendre points, N_{npe} is the number of nodes per element, and C_{int} is the complexity of recursive integration.

Once the coefficient matrix **A** is obtained, the transfer matrix **E** is calculated by solving the matrix Eq. (4) for m different right hand side vectors. At this stage, the total number of matrix-vector multiplications is $m \times i$ where i denotes the number of iterations that depends on the mesh size and the KSM used.

To calculate Φ_3^0 for a given source configuration, inverse of the sub-matrix $\mathbf{A}_s$ is required [29]. In this study, $\mathbf{A}_s^{-1}$ is computed using the generalized minimal residual (GMRES) [43] algorithm. Consequently, the computational complexity in calculating $\mathbf{A}_s^{-1}$ becomes $2N^2 \times N_{\text{mv}} \times m$, where N_{mv} is the number of matrix-vector multiplications. It is noted that, this phase of the accelerated BEM approach appears to be the main computational load of the FP solution.

2.2.2 Accelerated BEM for MEG

To obtain the MEG transfer matrix **M**, the same coefficient matrix **A** is required. Thus, once **A** is computed it can be used for the computation of both transfer matrices.

The next step in the calculation of **M** is the solution of (6) using n different vectors $\mathbf{h}_i$ on the right hand side. The number of matrix-vector multiplications of this phase is $m \times i$, where i denotes the number of iterations that depends on the mesh size and the KSM used.

The computational complexity for Φ_3^0 is given in the previous subsection. To incorporate IPA, an additional matrix-vector multiplication is required. This brings flops proportional to $m \times N_{\text{br}}$, where N_{br} is the number of the nodes on the inner skull boundary [2].

2.3 Parallel implementation of the accelerated BEM approach

2.3.1 Data partitioning

The purpose of using a parallel cluster is twofold: (1) to reduce the computation time, and (2) to combine the memory and storage resources of the *computing nodes* (computers). As a result, using a parallel cluster makes it possible to solve large sized problems, which would otherwise cause running out of memory on a single workstation. When the problem is distributed into the cluster, the following data are considered:

Mesh data: The mesh data consists of the node coordinates and element connectivity information. It is used during the construction of the coefficient matrix **A**. The BEM coefficient matrices are dense, i.e., each node contributes to the potential of any other node. To provide faster processing in matrix filling, mesh information must be kept on each processor.

Coefficient matrix **A**: For the accelerated BEM approach, the transpose of the coefficient matrix is required in Eq. (4). This matrix is computed and stored row-by-row on each processor.

Sub-matrix $\mathbf{A}_s$: When IPA is used, the coefficient matrix for the inner mesh ($\mathbf{A}_s$) is required to compute the modified right-hand-side vectors [29]. In this study, the rows of $\mathbf{A}_s$ is computed directly at each processor and an iterative solution is obtained for each source configuration.

The transfer matrices: The IP of EMSI requires successive matrix-vector multiplications using **E**, and for faster operations, this matrix must be distributed among the processors. For this purpose, each row of **E** is collected from all the processors to the appropriate processor. We preferred a row-based matrix distribution since the additional communication burden is not significant as long as the number of nodes, N, is larger than the number of processors, N_{np}. In this study, the number of processors is 8 and the number of nodes is at least 12,294. Thus, the communication overhead is acceptable.

2.3.2 Constructing the transfer matrix

The PETSc library distributes matrices among the processors as sets of rows. Since the parallel cluster is

homogeneous, each processor keeps equal number of successive rows. For optimum performance, each processor should compute its corresponding rows, minimizing inter-processor communication time.

Using the BEM formulation given in the previous section, each row of the BEM coefficient matrix $\mathbf{A}$ can be constructed independently. For problems where the number of nodes is significantly larger than the number of processors, such a matrix filling scheme may provide a speed-up which is proportional to the number of processors. This is the case for the sub-matrix $\mathbf{A}_s$ used by the IPA. On the other hand, computation of the transfer matrices require $\mathbf{A}^T$. Since obtaining the transpose of a matrix is an expensive operation, we preferred to construct $\mathbf{A}^T$ directly. Unfortunately, constructing $\mathbf{A}^T$ row-by-row, with minimal inter-processor communication is not straightforward. The source nodes are distributed among the processors, and contribution of source nodes to the potential at a specific field node is obtained through the surface integrals. Standard matrix filling procedure, where each element is processed sequentially for each field node, results in multiple access to each source node, at a random sequence. This process becomes inefficient when the source nodes are distributed, since either additional communication or redundant computation is required to fill the matrix. Thus, for efficient computation, a more complicated filling scheme is applied.

The filling scheme is based on selecting the elements-to-process in an intelligent way to avoid redundant computation due to multiple visits to an element. For that purpose, for each source node, the elements that the node is connected are processed. On each of these elements, the corresponding matrix entries in the rows owned by the processor are calculated and set according to the numerical integration on the element. Thus, contribution of each element node is added to the row and column of the field node. The element is then marked as "visited" to avoid future visits. While this scheme prevents idle or inefficient element visits and eliminates inter-processor communication, some redundant computation occurs due to elements having nodes in more than one processor.

Speed-up in filling the system matrix $\mathbf{A}$ strictly depends on the mesh representation. It is possible to improve the speed-up in matrix generation by modifying the initial mesh ordering. To avoid redundant element visits during matrix filling, the nodes must be reordered so that the nodes of each element take nearby indices. The elements must also be ordered so that neighboring elements have nearby indices. Such a mesh representation is obtained as follows:

1. The nodes of each boundary are sorted according to their z-coordinates.
2. The new indices are updated in the element data.
3. The elements are sorted according to the indices of their nodes.
4. The meshes of different boundaries are merged (concatenated).

2.3.3 *The parallel computation cluster*

Figure 1 illustrates the present configuration of the cluster named *Marvin*. The four Nodelin workstations are connected to each other over a 100 Mb/s Ethernet switch and the Athlin nodes are connected to each other over a Gigabit Ethernet switch. All cluster nodes are running under the Linux operating system. The controlling workstation is running FreeBSD and provides access to the cluster nodes.

The computation nodes have the following libraries for parallel processing and numerical operations: message passing interface (MPI) [25], automatically tuned linear algebra subroutines (ATLAS) version [46] of basic linear algebra subprograms (BLAS) [32], linear algebra package (LAPACK) [3], and PETSc [5]. These libraries are organized in a layered structure, in which the PETSc is the topmost layer.

3 Results

3.1 Head models

Meshes are generated from 72-slice segmented MR images. The meshes are constructed using a semi-automatic mesh generation algorithm [2]. For this purpose, first the segmented volume is triangulated using the skeleton climbing algorithm [40] then it is coarsened until the desired number of elements is obtained [28]. Figure 2 shows a fine mesh (with 30,000 nodes).

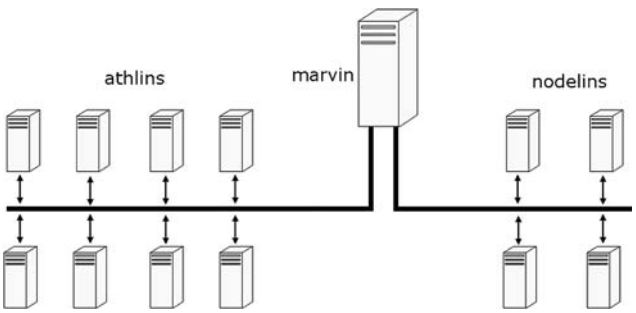

Fig. 1 The Marvin cluster structure. The cluster is composed of two groups: athlins have single AMD 2,500+ (1,833 MHz) processors on each PC (1.5 GB RAM), nodelins have dual PIII (933 MHz) processors on each PC

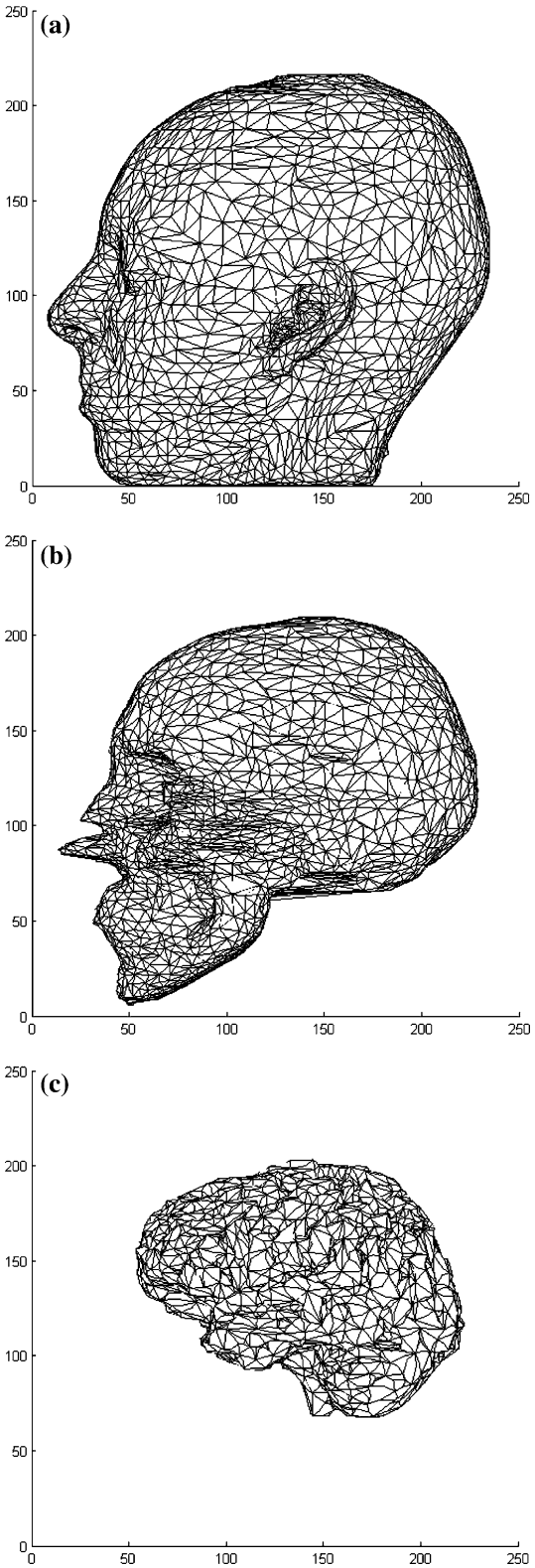

Fig. 2 A fine head model (30,000 nodes): **a** scalp (10,002 nodes, 5,000 elements), **b** skull (10,001 nodes, 4,999 elements), **c** brain (9,796 nodes, 5,000 elements)

3.2 Assessment of accuracy

The accuracy in the FP solutions was tested in [2, 21]. In the present study, the parallel version of the accelerated BEM approach is tested using a spherical three-layer Rush and Driscoll model [42]. In this model, the radii of the brain, skull and scalp surfaces are 8, 8.5 and 9.2 cm and the corresponding conductivities are 0.2, 0.0025 and 0.2 S/m, respectively. The accuracy for tangentially and radially oriented dipoles at varying depths are tested with the analytical solutions [45]. The results are the same with the ones presented for a single-processor implementation [2].

3.3 Performances of the KSMs

The computation times for various KSMs are explored for different number of processors. For this purpose, the three-layer Rush and Driscoll head model (with 12,294 nodes and 6,144 elements) is used. Then the matrix Eq. (4) is solved by each KSM with different number of processors. Table 1 presents the average solution times for various KSMs.

It is observed that, the GMRES method has the best performance among the evaluated KSMs. This is an expected result since GMRES is generally the most robust method for dense matrix equations. Preconditioning improves the convergence (the number of iterations before convergence reduces), but not the convergence time. These results are consistent with the ones reported in [41].

In the computation process of $\mathbf{E}$, a non-zero initial guess for each row ($\mathbf{e_i}$) greatly improves the convergence. This is due to the diagonally dominant characteristic of $\mathbf{A}$ (and $\mathbf{A}^{-1}$).

Table 1 Solution times (in seconds) for different KSMs using different number of processors

Processors	GMRES	Bi-CGSTAB	CGS	TFQMR	CR	CGNE
1	93.16	112.29	124.36	114.62	151.16	1,120.01
2	42.87	45.86	50.51	50.21	66.91	469.82
3	41.45	48.75	49.85	49.42	65.55	462.18
4	20.57	25.36	24.71	24.57	34.18	248.97
5	17.09	20.43	16.44	16.67	22.49	169.24
6	16.48	20.46	19.70	16.98	23.98	157.94
7	12.50	14.39	14.47	13.31	19.50	147.69
8	10.99	13.10	13.18	13.16	18.11	137.02

GMRES generalized minimal residual, *Bi-CGSTAB* bi-conjugate gradients stabilized, *CGS* conjugate gradients squared, *TFQMR* transpose-free quasi-minimal residual, *CR* conjugate residuals, *CGNE* conjugate gradient on normalized equations. A three-layer concentric sphere head model of 12,294-nodes is assumed

In this implementation, the initial estimate is selected as the right-hand side vector.

3.4 Speed-up

When the FP solutions are obtained using large number of nodes with a single processor, computation time and memory requirements increase. For a mesh of 30,000 nodes, for instance, the system matrix contains 900 million double precision entries, which corresponds to 7.2 GB of memory. Since each node in the parallel cluster has 1.5 GB of memory, this memory requirement can only be supplied by five or more nodes of the cluster. Thus, to compute speed-up figures for the full range of processors, a small three-layer spherical model with 12,294 nodes is used. The performance of parallelization is also tested for the two realistic head models (the fine mesh is presented in Fig. 2, and referred as Mesh 2 in Table 2). The parallelization performance of various stages are presented in Fig. 3. These

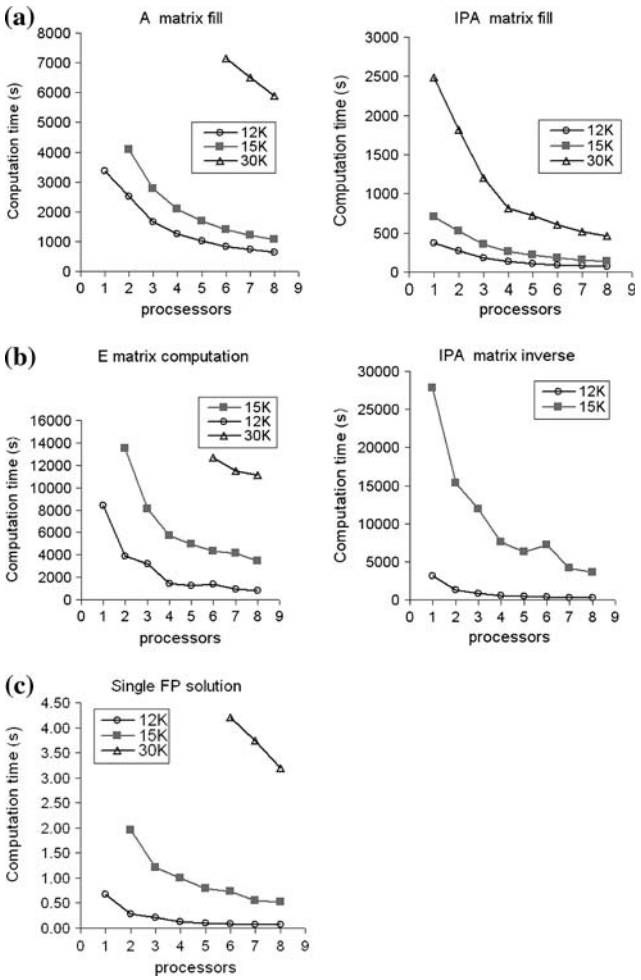

Fig. 3 Test of parallelization efficiency using spherical and realistic models. **a** Filling **A** and $\mathbf{A}_s$, **b** computation of **E** and $\mathbf{A}_s^{-1}$, and **c** computation of single FP solutions

Table 2 Efficiency of parallelization in various phases of the BEM implementation

Mesh	$\mathbf{A_s}$ fill (%)	$\mathbf{A}_s^{-1}$ computation (%)	**A** fill (%)	**E** computation (%)	Single FP solution (%)
Spherical	65.8	131.5	66.4	127.9	117.4
Mesh 1	65.6	96.6	95.3	97.5	94.2
Mesh 2	67.7	–	91.2	85.8	98.7

stages are: (1) filling the system matrix, (2) construction of the transfer matrix **E**, (3) solution of the isolated problem, (4) computation of the modified right hand side vector $\mathbf{g}'$ and (5) obtaining the potential distribution by $\mathbf{Eg}'$.

For the spherical (12,294 node) and the coarse realistic (Mesh 1:15,011 node) meshes, the speed-up assessment for filling **A** and **E** matrices is performed by taking the two-processors experiment as the reference, instead of the one with single-processor experiment. The reason for this choice is the swap space used in the single-processor case, which slows down the computations.

The speed-up efficiency (speed-up/number of processors) varies for different phases of the FP solution process. As expected, efficiency drops for increased number of processors. The efficiency values for the spherical and realistic models are presented in Table 2. The efficiency values for matrix filling get their values at the transition from single-processor to two-processors case (the library switches to parallel mode) and remain very close to these values for increased number of processors. For the cases where the single-processor data are not available, the efficiency values are very close to 100%. For instance, the computation time with two processors is approximately four times longer than that of eight processors case.

4 Discussion

In solving the EMSI IP, many FP solutions are required. Thus, once the coefficient and transfer matrices are computed, the speed-up in the FP solution becomes important. Note that, once the transfer matrix, **E**, is calculated, it can be used on a single-processor to compute the FP solutions. This is possible because the transfer matrix **E** uses much less memory, compared with the coefficient matrix **A**, and fits the memory of a single node. When the linear approach is used for the IP solutions, the FP is solved for a large number of source locations. In such as case, it is possible to split the source space among the processors. Each node then solves the FP for the assigned dipoles with 100% efficiency. Thus, the choice of the IP approach should determine the technique used in the FP solutions.

Each phase of FP solution yields different efficiency (speed-up/number of processors) figures. Note that some efficiency figures are greater than 100%. These super-linear efficiency values are explained by cache scaling. With increased number of processors, the total amount of available processor cache increases and more data is processed on these fast memory units resulting in faster operation.

When spatio-temporal behavior of the sources is of interest, the number of IP solutions is equal to the number of samples taken from EEG/MEG recordings. An increase in the temporal resolution requires more operations, yielding longer computation time. For a single-processor case, the IP computations may take hours, even for a single instant.

Parallelization provides the ability to combine the memory resources of all nodes. When solved on a single node, the realistic meshes used in this study consumes all the memory and start using swap space, further slowing down the computation. Since the coefficient matrix requires memory proportional to the square of the number of nodes, more computation nodes (memory) is required for large meshes. For instance, the 30 K node mesh requires more than five processors to be processed properly without using the swap space.

When incorporating the IPA, we preferred iterative solutions instead of calculating $\mathbf{A}_s^{-1}$. For the FP solutions, this choice increases the solution time for a given source configuration (from 32 to 72 ms for the 12 K mesh and from 41 to 520 ms for the 15 K mesh). Note that, inversion of $\mathbf{A_s}$ may take hours depending on the size of this matrix. Thus, for the IP, iterative IPA solution is computationally preferable if the number of FP solutions is much smaller than the number of nodes in $\mathbf{A_s}$. If this is not the case, the use of direct inversion or LU factorization will definitely be a better choice for the IPA solution.

The importance of IPA increases with the conductivity ratio around the inner-skull layer (β). For the numerical accuracy of the BEM formulation IPA must be used for β values smaller than 0.1 [29]. For the three layer head model used in this study, β corresponds to the skull/brain conductivity ratio. This ratio was assumed to be 1/80 which is the value measured by Rush and Driscoll [42], and later by Goncalves et al. [24]. Recent studies, however, report that this ratio is around 1/20 rather than 1/80 [31, 38, 48]. With this ratio, IPA is still required. The benefits of parallel implementation are valuable even if IPA is not required.

5 Conclusion

When the spatio-temporal behavior of electrical activities in the brain is explored for the clinical applications, the computation time is critical, and efficient parallelization is crucial. This study investigated the use of parallel processing in the solution of the EMSI FP with highly realistic head models. For this purpose, the accelerated BEM approach [2] was implemented using a Beowulf cluster with eight nodes (PC workstations).

Our main contributions are summarized as follows: (1) A feasible and scalable parallelization scheme is presented for the accelerated BEM approach. (2) The performance of the proposed parallelization scheme is tested. It was observed that our scheme provides memory scaling as well as faster operation with a considerable speed-up in the matrix filling, transfer matrix calculation and solution phases. (3) Some practical issues in parallelization are addressed. (4) The solution times for the resultant equations were compared for various KSMs and the fastest method (GMRES) is reported.

Acknowledgments This work is supported by the Middle East Technical University Research Fund Projects AFP-98-03-01-03, AFP-2001-03-01-02, BAP-2003-07-02-00-12, and BAP-2004-03-01-03.

Appendix: BEM formulation

The electric potential ϕ and the magnetic field $\mathbf{B}$ due to a current dipole source $\mathbf{p}$ in a piecewise homogeneous volume conductor model of the head, satisfy the following integral equations [23]:

$$\bar{\sigma}\phi(\mathbf{r}) = g(\mathbf{r}) + \frac{1}{4\pi}\sum_{k=1}^{L}(\sigma_k^- - \sigma_k^+)\int_{S_k}\phi(\mathbf{r}')\frac{\mathbf{R}}{R^3}\cdot d\mathbf{S}_k(\mathbf{r}'), \tag{7}$$

$$\mathbf{B}(\mathbf{r}) = \mathbf{B}_0(\mathbf{r}) + \frac{\mu_0}{4\pi}\sum_{k=1}^{L}(\sigma_k^- - \sigma_k^+)\int_{S_k}\phi(\mathbf{r}')\frac{\mathbf{R}}{R^3}\times d\mathbf{S}_k(\mathbf{r}'). \tag{8}$$

Here, the surfaces between different conductivity regions are denoted by S_k, $k = 1...L$. The inner and outer conductivities of S_k are represented by σ_k^- and σ_k^+, respectively. $\mathbf{R} = \mathbf{r}-\mathbf{r}'$ is the vector between the field point $\mathbf{r}$ and the source point $\mathbf{r}'$, and $\bar{\sigma}$ is the mean conductivity at the field point. The contribution of the primary sources, g and $\mathbf{B}_0$, are defined as follows:

$$g(\mathbf{r}) = \frac{1}{4\pi\sigma_0}\frac{\mathbf{p}\cdot\mathbf{R}}{R^3}, \tag{9}$$

$$\mathbf{B}_0(\mathbf{r}) = \frac{\mu_0\mathbf{p}\times\mathbf{R}}{4\pi\ R^3}, \tag{10}$$

where σ_0 is the unit conductivity and μ_0 is the permeability of the free space. Equations (7) and (8) can be solved numerically by dividing the surfaces into elements and computing the surface integrals over these elements [7–9, 23]. The surface elements used in this study are

triangular, quadratic and isoparametric. Using (7) for all nodes and integrating over all elements, a set of equations with N unknowns can be obtained (here N denotes the number of nodes in the BEM mesh). In matrix notation, this can be expressed as:

$$\begin{aligned} \Phi &= \mathbf{g} + \mathbf{C}\Phi \\ (\mathbf{I} - \mathbf{C})\Phi &= \mathbf{g} \\ \mathbf{A}\Phi &= \mathbf{g} \end{aligned} \tag{11}$$

where Φ is an $N \times 1$ vector of node potentials, $\mathbf{C}$ is an $N \times N$ matrix whose elements are determined by the geometry and electrical conductivity of the head and $\mathbf{g}$ is an $N \times 1$ vector representing the contribution of the primary sources. Φ is then obtained as:

$$\Phi = \mathbf{A}^{-1}\mathbf{g} \tag{12}$$

To eliminate the singularity in the coefficient matrix $\mathbf{A}$, the method of matrix deflation is employed [33]. IPA is implemented to overcome numerical errors caused by high conductivity difference around the skull layer [29]. Once Φ is computed, $\mathbf{B}$ is calculated from the potential values using (8). In matrix notation this can be written as follows:

$$\mathbf{B} = \mathbf{B_0} + \mathbf{H}\Phi \tag{13}$$

If the number of magnetic sensors is m, $\mathbf{B}$ is an $m \times 1$ vector representing the magnetic fields at the sensor locations, and $\mathbf{B_0}$ denotes the $m \times 1$ vector of magnetic fields at the same sensor locations for an unbounded homogeneous medium. Here, $\mathbf{H}$ is an $m \times N$ coefficient matrix determined by the geometry and electrical conductivity of the head.

References

1. Acar CE (2003) Parallelization of the forward and inverse problems of electromagnetic source imaging of the human brain. Ph.D. thesis, Middle East Technical University, Ankara, Turkey
2. Akalın-Acar Z, Gençer NG (2004) An advanced boundary element method implementation for the forward problem of electromagnetic source imaging. Phys Med Biol 49(21):5011–5028
3. Anderson E, Bai Z, Bischof C, Blackford S, Demmel J, Dongarra J, Du Croz J, Greenbaum A, Hammarling S, McKenney A, Sorensen D (1999) LAPACK users' guide, 3rd edn. Society for Industrial and Applied Mathematics, PA, ISBN 0-89871-447-8
4. Baillet S, Mosher JC, Leahy MR (2001) Electromagnetic brain mapping. IEEE Signal Process Mag 18(6):14–30
5. Balay S, Eijkhout V, Gropp WD, McInnes LC, Smith BF (1997) Efficient management of parallelism in object oriented numerical software libraries. In: Arge E, Bruaset AM, Langtangen HP (eds) Modern software tools in scientific computing. Birkhäuser Press, Germany, pp 163–202
6. Baltz BA, Ingber MS (1997) A parallel implementation of the boundary element method for heat conduction analysis in heterogeneous media. Eng Anal Bound Elem 19:3–11
7. Barnard AC, Duck IM, Lynn MS (1967) The application of electromagnetic theory to electrocardiology: I. Derivation of the integral equations. Biophys J 7:443–462
8. Barnard AC, Duck IM, Lynn MS, Timlake WP (1967) The application of electromagnetic theory to electrocardiology: II. Numerical solution of the integral equations. Biophys J 7:463–491
9. Barr RC, Pilkington TC, Boineau JP, Spach MS (1966) Determining surface potentials from current dipoles, with application to electrocardiography. IEEE Trans Biomed Eng 13:88–92
10. Barrett R, Berry M, Chan TF, Demmel J, Donato J, Dongarra J, Eijkhout V, Pozo R, Romine C, Van der Vorst H (1994) Templates for the solution of linear systems: building blocks for iterative methods, 2nd edn. SIAM, Philadelphia. http://www.netlib.org/linalg/html_templates/report.html
11. Beowulf cluster site http://www.beowulf.org/
12. Cowper GR (1973) Gaussian quadrature formulas for triangles. Int J Num Methods Eng 7:405–408
13. Crouzeix A, Yvert B, Bertrand O, Pernier J (1999) An evaluation of dipole reconstruction accuracy with spherical and realistic head models in MEG. Clin Neurophysiol 110:2176–2188
14. Cuffin BN (1996) EEG localization accuracy improvements using realistically shaped head models. IEEE Trans Biomed Eng 44:299–303
15. Cuffin BN (1998) EEG dipole source localization. IEEE Eng Med Biol 17(5):118–122
16. DeMunck JC, van Dijk BW, Spekreijse H (1988) Mathematical dipoles are adequate to describe realistic generators of human brain activity. IEEE Trans Biomed Eng 35(11):960–966
17. Frijns JHM, de Snoo SL, Schoonhoven R (2000) Improving the accuracy of the boundary element method by the use of second-order interpolation functions. IEEE Trans Biomed Eng 47(10):1336–1346
18. Fuchs M, Drenckhahn R, Wischmann HA, Wagner M (1998) An improved boundary element method for realistic volume-conductor modeling. IEEE Trans Biomed Eng 45(8):980–997
19. Gençer NG, Acar CE, Tanzer IO (2003) Forward problem solution of magnetic source imaging. In: Lu ZL, Kaufman L (eds) Magnetic source imaging of the human brain. Lawrence Erlbaum Associates, Hillsdale
20. Gençer NG, Acar CE (2004) Sensitivity of EEG and MEG measurements to tissue conductivity. Phys Med Biol 49:701–717
21. Gençer NG, Tanzer IO (1999) Forward problem solution of electromagnetic source imaging using a new BEM formulation with high-order elements. Phys Med Biol 44:2275–2287
22. Gençer NG, Akalın-Acar Z (2005) Use of the isolated problem approach for multi-compartment BEM models of electro-magnetic source imaging. Phys Med Biol 50:3007–3022
23. Geselowitz DB (1967) On bioelectric potentials in an inhomogeneous volume conductor. Biophys J 7:1–11
24. Goncalves S, de Munck JC, Verbunt JPA, Heethaar RM, da Silva FHL (2003) In vivo measurement of the brain and skull resistivities using an EIT-based method and realistic models for the head. IEEE Trans Biomed Eng 50(6):75467
25. Gropp W, Lusk E, Doss N, Skjellum A (1996) A high-performance, portable implementation of the MPI message passing interface standard. Parallel Comput 22(6):789–828
26. He B (1998) High-resolution source imaging of brain electrical activity. IEEE Eng Med Biol 17(5):123–129
27. He B, Musha T, Okamoto Y, Homma S, Nakajima Y, Sato T (1987) Electric dipole tracing in the brain by means of the boundary element method and its solution accuracy. IEEE Trans Biomed Eng 34:406–414
28. Heckbert PS, Garland M (1999) Optimal triangulation and quadric-based surface simplification. Computat Geom 14:49–65

29. Hämäläinen MS, Sarvas J (1989) Realistic conductivity geometry model of the human head for interpretation of neuromagnetic data. IEEE Trans Biomed Eng 36(2):165–171
30. Kreienmeyer M, Stein E (1997) Efficient parallel solvers for boundary element equations using data decomposition. Eng Anal Bound Elem 19:33–39
31. Lai Y, van W. Drongelen, Ding L, Hecox KE, Towle VL, Frim DM, He B, (2005) In vivo human skull conductivity estimation from simultaneous extra- and intra-cranial electrical potential recordings. Clin Neurophysiol 116(2):456–465
32. Lawson CL, Hanson RJ, Kincaid D, Krogh FT (1979) Basic linear algebra subprograms for FORTRAN usage. ACM Trans Math Soft 5:308–323
33. Lynn MS, Timlake WP (1968) The use of multiple deflations in the numerical solution of singular systems of equations, with applications to potential theory. SIAM J Numer Anal 5:303–322
34. Meijs JWH, Weier O, Peters MJ (1989) On the numerical accuracy of the boundary element method. IEEE Trans Biomed Eng 36:1038–1049
35. Mohr M, Vanrumste B (2003) Comparing iterative solvers for linear systems associated with the finite difference discretisation of the forward problem in electro-encephalographic source analysis. Med Biol Eng Comput 41(1):75–84
36. Mosher JC, Leahy RM, Lewis PS (1999) EEG and MEG: forward solutions for inverse methods. IEEE Trans Biomed Eng 46(3):245–259
37. Natarajan R, Krishnaswamy D (1995) A case study in parallel scientific computing: the boundary element method on a distributed-memory multicomputer. In: Proceedings, ACM/IEEE conference on supercomputing
38. Oostendorp TF, Delbeke J, Stegeman DF (2000) The conductivity of the human skull: results of in vivo and in vitro measurements. IEEE Trans Biomed Eng 47(11):1487–1492
39. Pinto B, Quintao Silva C (2007) A simple method for calculating the depth of EEG sources using minimum norm estimates (MNE). Med Biol Eng Comput 45(7):643–652
40. Poston T, Wong T, Heng P (1998) Multiresolution isosurface extraction with adaptive skeleton climbing. In: Proc. of eurographics '98, p 17
41. Rahola J, Tissari S (2002) Iterative solution of dense linear systems arising from the electrostatic integral equation in MEG. Phys Med Biol 47:961–975
42. Rush S, Driscoll DA (1969) EEG electrode sensitivity-an application of reciprocity. IEEE Trans Biomed Eng 16:15–22
43. Saad Y, Schultz MH (1986) GMRES: a generalized minimal residual algorithm for solving nonsymmetric linear systems. SIAM J Sci Stat Comput 7:856–869
44. Song SW, Baddour RE (1997) Parallel processing for boundary element computations on distributed systems. Eng Anal Bound Elem 19:73–84
45. Stok CJ (1986) The inverse problem in EEG and MEG with application to visual evoked responses, pp 101–117, ISBN 90-70647-06-0
46. Whaley RC, Petitet A, Dongarra JJ (2001) Automated empirical optimization of software and the ATLAS project. Parallel Comput 27(1–2):3–35
47. Wolters CH, Grasedyck L, Hackbusch W (2004) Efficient computation of lead field bases and influence matrix for the FEM-based EEG and MEG inverse problem. Inverse Probl 20:1099–1116
48. Zhang Y, van Drongelen W, He B (2006) Estimation of in vivo brain-to-skull conductivity ratio in humans. Appl Phys Lett 89:223903–2239033